

Synthesis of Titanate Nanotube–CdS Nanocomposites with Enhanced Visible Light Photocatalytic Activity

Zi-Rong Tang,^{*,†} Xia Yin,[†] Yanhui Zhang,^{†,‡} and Yi-Jun Xu^{†,‡}

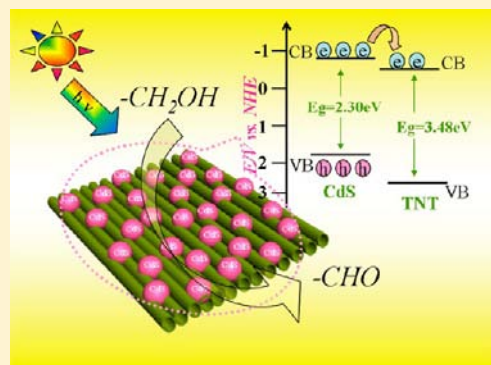
[†]College of Chemistry and Chemical Engineering, New Campus, Fuzhou University, Fuzhou 350108, People's Republic of China

[‡]State Key Laboratory Breeding Base of Photocatalysis, College of Chemistry and Chemical Engineering, Fuzhou University, Fuzhou, 350002, People's Republic of China

Supporting Information

ABSTRACT: CdS–1D titanate nanotubes (CdS/TNTs) nanocomposites have been synthesized via a facile one-step in situ hydrothermal method. The structure and properties of CdS/TNTs nanocomposites have been characterized by X-ray diffraction, UV–vis diffuse reflectance spectra, transmission electron microscopy, photoluminescence spectra, nitrogen adsorption–desorption, and electron spin resonance spectra. The results show that (i) as compared to blank-CdS, it is found that the morphology of CdS in the CdS/TNTs nanocomposites can be finely tuned by TNTs formed during the one-step in situ hydrothermal process; and (ii) the CdS/TNTs nanocomposites exhibit remarkably much higher visible light photocatalytic activity than both blank-CdS and blank-TNT toward aerobic selective oxidation of alcohols under mild conditions. Three integrative factors lead to such a drastic photoactivity enhancement for CdS/TNTs nanocomposites.

The first one is the different morphology of CdS in the CdS/TNTs nanocomposites from blank-CdS. The second one is the prolonged lifetime of photogenerated electron–hole pairs from CdS in CdS/TNTs nanocomposites under visible light irradiation. The third one is the higher surface area and adsorption capacity of CdS/TNTs nanocomposites than blank-CdS. In addition, the possible reaction mechanism for photocatalytic selective oxidation of alcohols over CdS/TNTs nanocomposites has also been investigated using the radical scavengers technique. It is hoped that this work could promote further interest in fabrication of various 1D TNT-based composite materials and their application to visible-light-driven photocatalytic selective organic transformations.



INTRODUCTION

One-dimensional (1D) semiconducting nanostructures, such as nanotubes, nanorods and nanowires have been the focus of considerable attention because of their unique structural and electronic properties. So far, they have been widely used in a variety of fields, such as photodetectors, light waveguides, solar cells, lithium batteries, gas sensing, and photocatalysis.^{1–10} Especially, one-dimensional titanate nanotubes (TNTs) as photocatalyst have been remaining a subject of many investigations,^{11–24} such as degradation of pollutants,^{11–18,23} hydrogen production,^{19–22} and selective organic transformation,²⁴ due to their following promising features from a viewpoint of photocatalysis. First, the 1D geometry facilitates fast and long-distance electron transport. Second, the 1D nanotubular structure is expected to have a large specific surface area and pore volume. Third, the light absorption and scattering can be markedly enhanced because of the high length-to-diameter ratio for 1D nanotubular TNTs. For example, our group has utilized the 1D TNTs as photocatalyst for degradation of aromatic pollutant benzene in the gas phase, which shows that the 1D TNTs can exhibit enhanced photoactivity as compared to commercial P25-TiO₂ nanoparticles under ultraviolet (UV) light irradiation.¹⁸ More

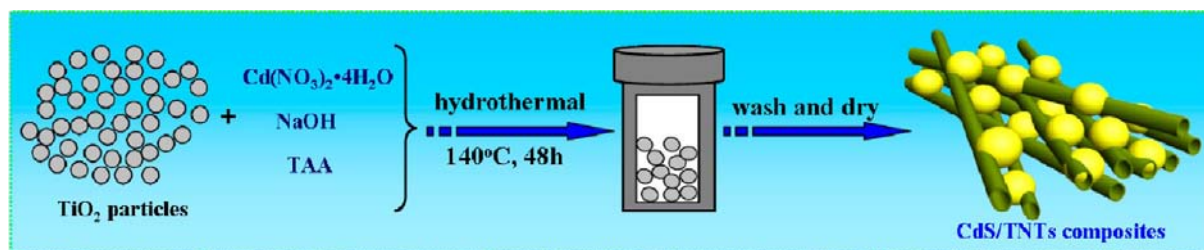
recently, we have reported that doping metal ions into the framework of TNTs endows it with visible light photoactivity and enhanced UV light photoactivity toward selective oxidation of alcohols under ambient conditions.²⁴

Notably, there are two obvious drawbacks of the 1D TNTs photocatalyst.^{11–24} On one hand, TNT is a wide band gap semiconductor that restricts the photoresponse of the only UV region with the wavelength below 390 nm, thus significantly depressing the visible light utilization of the solar spectrum. On the other hand, the high rate of photogenerated electron–hole pair recombination in TNTs under UV light irradiation results in low quantum efficiency of photocatalytic reactions. Therefore, extending the optical absorption of TNTs into the visible light region and increasing the photoactivity of TNTs are of great interest for the practical application of TNTs or TNT-based semiconductor materials toward target photocatalytic reactions. To date, a variety of strategies have been utilized to improve the performance of TNTs, including doping TNTs with a metal or nonmetal^{18,24–27} and coupling with organic dye or narrow band semiconductors, such as CdS,^{28–39} CdSe,^{40,41}

Received: April 26, 2013

Published: September 27, 2013

Scheme 1. Illustration for Preparation of CdS/TNTs Nanocomposites by One-Step in Situ Hydrothermal Process



and CdTe.^{42,43} For example, our group has recently reported that metal-ion doping can extend the light absorption range of TNTs to the visible light region. The as-obtained metal-ion-doped TNTs show enhanced photoactivity toward selective oxidation of alcohols under both UV and visible light irradiation.²⁴ However, they still have relatively low photocatalytic activity. Thus, besides doping strategies, it is highly desirable to adopt other approaches to modify the 1D TNTs semiconductor toward significantly improved photoactivity for selective oxidation of alcohols. In this regard, it is worth noting that increasing efforts are focused on coupling TNTs with CdS to form efficient composite photocatalysts,^{44–50} because CdS is an important narrow band gap semiconductor, which can sensitize wide band gap TNTs and thus modulate the photoresponse to the visible light spectrum. In addition, the energy band position of TNTs allows for the transfer of photogenerated electrons from CdS to the conduction band of TNTs, which could further boost the fate and transfer of photogenerated charge carriers that would consequently contribute to the photoactivity enhancement.

So far, TNTs modified by CdS nanoparticles have been realized by means of various strategies, such as ion-exchange reaction,^{47–49} employing sulfur powder and Cd²⁺ in dimethyl sulfoxide,⁵⁰ and sequential chemical bath deposition.^{34,45} However, all previous research works on the CdS/TNTs nanocomposites are primarily focused on the photocatalytic applications in water splitting to hydrogen^{35,44,49} and degradation of organic pollutants, for example, azo dyes.^{11,45,47} To the best of our knowledge, there is no report on utilizing CdS/TNTs composites as a visible-light-driven photocatalyst toward photocatalytic organic transformation via selective oxidation under ambient conditions.^{24,51,52}

Herein, we report a facile one-step in situ hydrothermal method to fabricate CdS–1D titanate nanotubes (CdS/TNTs) nanocomposites during which the formation of the 1D nanostructure of TNTs and CdS nanoparticles is obtained simultaneously. In particular, we show for the first time that CdS/TNTs nanocomposites exhibit remarkable visible light photoactivity enhancement toward aerobic selective oxidation of benzylic alcohols and allylic alcohols under ambient conditions, which is an important synthetic reaction of industrial importance.^{24,51–57} The results show that, as compared to blank-CdS, the morphology of CdS can be tuned by the formation of TNTs in such an in situ synthesis of CdS/TNTs while the 1D nanostructure of TNTs is not influenced as compared to blank-TNT. Under visible light irradiation, the photogenerated electrons from CdS are able to transfer to the conduction band of TNTs, thus facilitating the efficient separation of charge carriers, which contributes to the drastic photoactivity improvement of CdS/TNTs nanocomposites for oxidation of alcohols. It is anticipated that this work could advance further interest on the fabrication of various 1D

TNTs-based nanocomposite materials for visible-light-driven selective organic transformations.

EXPERIMENTAL SECTION

Preparation. Materials. The chemicals sodium hydroxide (NaOH), cadmium nitrate ($\text{Cd}(\text{NO}_3)_2 \cdot 4\text{H}_2\text{O}$), and thioacetamide (TAA) were obtained from Sinopharm Chemical Reagent Co., Ltd. (Shanghai, China). Anatase titania nanosized powder (10 nm in size) was supplied from Alfa Aesar Co., Ltd. (Tianjin, China). All of the chemicals are analytic grades and used as received without further purification. Deionized water used in the synthesis was from local sources.

Synthesis. Synthesis of Blank-TNT. For the synthesis of TNTs, anatase titania powder (0.5 g) and an aqueous solution of concentrated NaOH (10 M, 40 mL) were mixed and kept stirring to form a homogeneous suspension, which was then transferred into a Teflon-lined autoclave and hydrothermally treated at 140 °C for 48 h in an oven. After the reaction, the precipitate was separated by filtration and washed with deionized water until the pH was neutral. Finally, the sample was dried in an oven at 60 °C.

Fabrication of CdS/TNTs Nanocomposites. The one-step synthesis of CdS/TNTs nanocomposites is based on a modified hydrothermal method.⁴⁴ The preparation process is illustrated in Scheme 1. Briefly, anatase titania powder (0.5 g) was first added to 40 mL of NaOH (10 M) solution. After stirring for 30 min, appropriate amounts of $\text{Cd}(\text{NO}_3)_2 \cdot 4\text{H}_2\text{O}$ (0.3856 g, 1.25 mmol) and excess TAA (0.1033 g, 1.37 mmol) were subsequently added to the suspension. The mixture was stirred for 30 min vigorously and then transferred to a 50 mL Teflon-lined stainless steel autoclave. The hydrothermal treatment was conducted at 140 °C for 48 h. After the reaction, the precipitate was separated by filtration and washed with deionized water until the pH was neutral. Finally, the sample was dried in an oven at 60 °C, by which CdS/TNTs nanocomposites were obtained; the weight ratio of CdS is 36% in the nanocomposite of CdS/TNTs in order to obtain the optimal photocatalytic performance.

Synthesis of Blank-CdS. The preparation process was the same as that for CdS/TNTs nanocomposites except that no anatase titania powder was added.

Characterization. The crystalline structure of the samples was determined by the powder X-ray diffraction (XRD, Philip X' Pert Pro MPP) using a Cu K α radiation in the 2θ ranging from 5° to 80° with a scan rate of 0.08°/s. The optical properties of the samples were analyzed by UV–vis diffuse reflectance spectroscopy (DRS) using a Cary-500 spectrophotometer over a wavelength range of 200–800 nm, during which BaSO₄ was employed as the internal reflectance standard. Field-emission scanning electron microscopy (FESEM) was used to determine the morphology of the samples on an FEI Nova NANOSEM 230 spectrophotometer. Transmission electron microscopy (TEM) images were obtained using a JEOL mode JEM 2010 EX instrument at the accelerating voltage of 200 kV. The particle size distribution was performed using a Nano measurer software. The photoluminescence (PL) spectra for all solid samples were investigated on a Cary Eclipse Fluorescence spectrophotometer with an excitation wavelength of 365 nm. To ensure the comparability of the PL spectra, the experimental parameters, including the excitation wavelength, slit width, and the amount of the samples, were identical. The electrochemical analysis was carried out in a conventional three-

electrode cell using a Pt plate and a Ag/AgCl electrode as the counter electrode and reference electrode, respectively. The electrolyte was 0.2 M Na₂SO₄ aqueous solution without additive (pH = 6.8). The working electrode was prepared on indium–tin oxide (ITO) glass that was cleaned by sonication in ethanol for 30 min and dried at 353 K. The boundary of ITO glass was protected using Scotch tape. The 10 mg sample was dispersed in 1 mL of ethanol by sonication to get a slurry. The slurry was spread onto the pretreated ITO glass. The working electrode was dried overnight under ambient conditions. Then, the Scotch tape was unstuck, and the uncoated part of the electrode was isolated with epoxy resin. The exposed area of the working electrode was 0.25 cm². The visible light irradiation source was a 300 W Xe arc lamp system equipped with a UV-CUT filter to cut off light of wavelength < 420 nm, which was the same light source as for the photoactivity test. The photocurrent measurements were taken on a BAS Epsilon workstation without bias. The electrochemical impedance spectroscopy (EIS) experiments were conducted on a Precision PARC workstation. Nitrogen adsorption–desorption isotherms were collected at 77 K over a Micromeritic-ASAP2020 equipment. The electron spin resonance (ESR) signal of the radicals spin-trapped by 5,5-dimethyl-1-pyrroline-*N*-oxide (DMPO) was measured using a Bruker EPR A300 spectrometer. Typically, the sample (5 mg) was dispersed in the solvent benzotrifluoride (0.5 mL). Then, 25 μL of DMPO/benzyl alcohol solution (1:10, v/v) was added and oscillated to achieve a well-blended suspension. The irradiation source (λ > 420 nm) was a 300 W Xe arc lamp system, the visible light source for our photocatalytic selective oxidation experiments as shown below.

Photocatalytic Activity Test. The photocatalytic selective oxidation of alcohols was carried out in a 10 mL Pyrex glass bottle under the irradiation of visible light, as performed in previous research works.^{24,58–62} In a typical process, a mixture of 8 mg of catalyst and 0.1 mmol of alcohols was dissolved in 1.5 mL of benzotrifluoride (BTF), which was saturated with pure molecular oxygen.^{24,58–62} The above mixture was transferred into a 10 mL Pyrex glass bottle and stirred for 10 min to make the catalyst blend evenly in the solution. The suspensions were irradiated by a 300 W Xe arc lamp (PLS-SXE 300, Beijing Perfectlight Co. Ltd.) with a UV–CUT filter to cut off light of wavelength λ < 420 nm. After the reaction, the mixture was centrifuged at 12 000 rpm for 20 min to completely remove the catalyst particles. The remaining solution was analyzed with an Agilent Gas Chromatograph (GC-7820 fitted with a FFAP capillary analysis column). Conversion, yield, and selectivity were defined as the following

$$\text{Conversion (\%)} = [(C_0 - C_{\text{alcohol}})/C_0] \times 100$$

$$\text{Yield (\%)} = C_{\text{aldehyde}}/C_0 \times 100$$

$$\text{Selectivity (\%)} = [C_{\text{aldehyde}}/(C_0 - C_{\text{alcohol}})] \times 100$$

where C₀ is the initial concentration of alcohol, and C_{alcohol} and C_{aldehyde} are the concentration of the substrate alcohol and the corresponding aldehyde, respectively, after the photocatalytic reaction.

RESULTS AND DISCUSSION

Figure 1 shows the powder X-ray diffraction (XRD) patterns of the samples of blank-TNT, CdS–1D titanate nanotubes (CdS/TNTs) nanocomposites, and blank-CdS. It can be seen that the peaks at 2θ values of 10.7, 24.5, 29.2, and 48.5° can be indexed to (200), (110), (211), and (020) crystal planes of the 1D TNT phase, respectively.^{18,24,63,64} The distinct diffraction peaks of blank-CdS at 2θ values of 24.8, 26.5, 28.2, 36.6, 43.7, 47.8, 51.8, 66.8, 72.4, and 77.9° correspond to the (100), (002), (101), (102), (110), (103), (112), (203), (114), and (204) facets of greenokite structure CdS (JCPDS 41-1049) with a hexagonal phase, respectively. Furthermore, the characteristic diffraction peaks assigned to TNTs and CdS can both be observed in the XRD pattern of CdS/TNTs nanocomposites, indicating the successful synthesis of the CdS/TNTs nano-

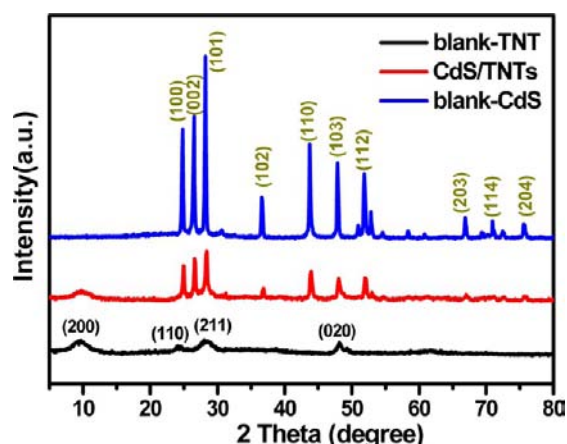


Figure 1. XRD patterns of blank-TNT, CdS/TNTs nanocomposites, and blank-CdS.

composites and that the 1D structure of TNTs is maintained.^{18,24} Notably, the intensity of diffraction peaks attributed to CdS in the CdS/TNTs nanocomposites is weaker than that of blank-CdS, which could be ascribed to two probable reasons. One is the relatively low content of CdS in the nanocomposite of CdS/TNTs. The other is due to that, during the in situ synthesis of CdS/TNT nanocomposites, the formation of 1D TNTs could affect the crystallinity of CdS. In addition, according to calculation from the (002) peak of the XRD pattern by the Scherrer formula, the average crystallite size of CdS particles in CdS/TNTs nanocomposites is about 26 nm, which is much smaller than 49 nm for blank-CdS. The XRD data clearly indicate that the crystallinity and crystallite size of CdS can be tuned by the formation of TNTs during one-step in situ hydrothermal synthesis of CdS/TNTs nanocomposites, which is remarkably different from the synthesis of blank-CdS.

The optical property measurement of blank-TNT, CdS/TNTs nanocomposites, and blank-CdS, using the UV–vis diffuse reflectance spectra (DRS), is shown in Figure 2. It can be seen from Figure 2a that the absorption edge of blank-TNTs is only located at the ultraviolet (UV) region below 390 nm, whereas the CdS/TNTs nanocomposites show an enhanced absorbance in the visible light region, although the light absorption intensity of CdS/TNTs nanocomposites is lower than that of blank-CdS. It is noted that the absorption edge of blank-TNT is located at below 390 nm, whereas blank-CdS shows a sharp absorption edge at around 550 nm. The introduction of CdS into the matrix of TNTs has a significant effect on the optical property for the CdS/TNTs nanocomposites. With the introduction of CdS content, there is an enhanced light absorbance in the visible light region for CdS/TNTs while the light absorption feature of TNT in the UV region (particularly at the wavelength of 300 nm) for the CdS/TNTs nanocomposite can still be clearly distinguished that is the same as that of blank-TNT. Thus, the light absorption spectrum of CdS/TNTs nanocomposites has the characteristic light absorption spectra of both blank-TNT and blank-CdS. A plot obtained via the transformation based on the Kubelka–Munk function versus the energy of light is shown in Figure 2b, by which the roughly estimated energy band gap (E_g) values are 3.48, 2.38, and 2.30 eV corresponding to blank-TNT, CdS/TNTs nanocomposites, and blank-CdS, respectively. The results of DRS indicate that the introduction of narrow band

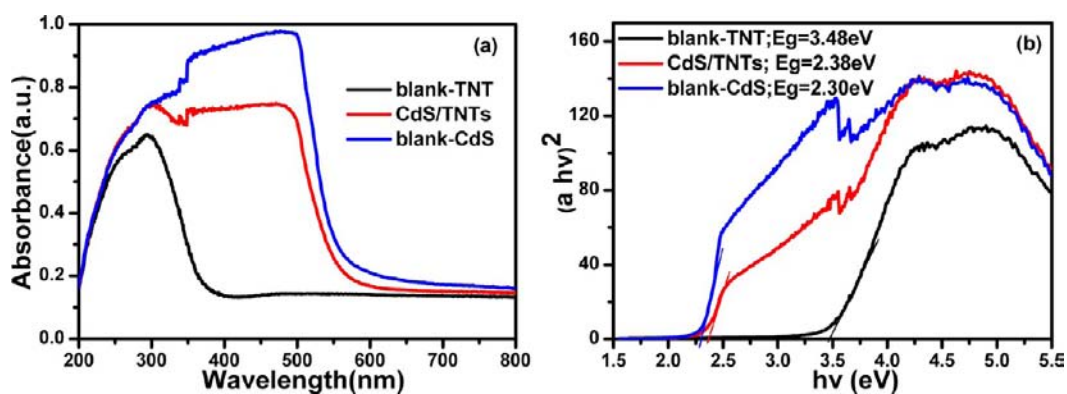


Figure 2. UV-vis diffuse reflectance spectra (DRS) of blank-TNT, CdS/TNTs nanocomposites, and blank-CdS (a), and the plot of transformed Kubelka–Munk function versus the energy of light (b).

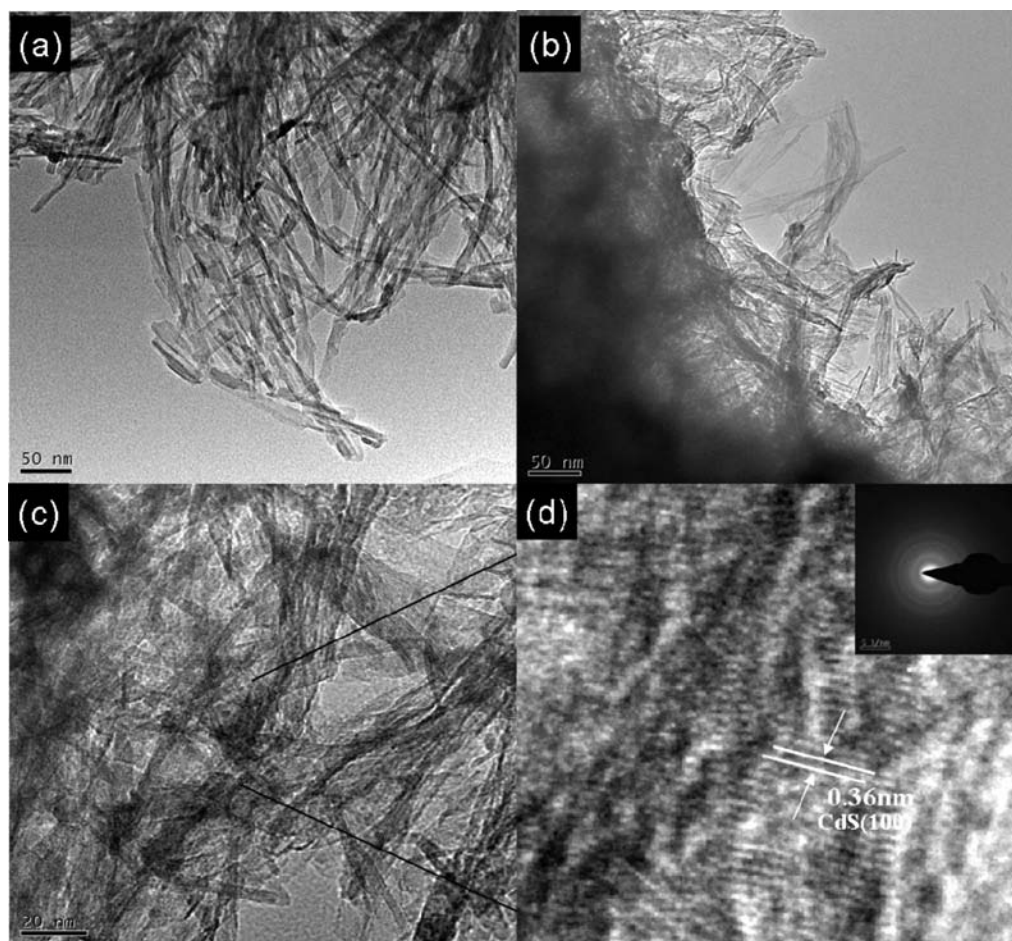


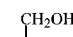
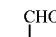
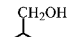
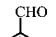
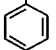
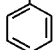
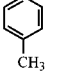
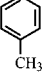
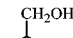
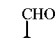
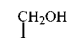
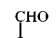
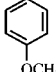
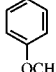
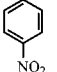
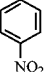
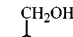
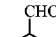
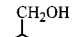
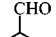
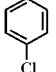
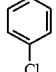
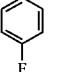
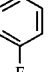
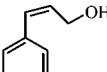
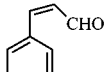
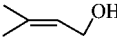
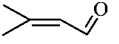
Figure 3. TEM images of blank-TNT (a) and CdS/TNTs nanocomposites (b, c) and HRTEM image of CdS/TNTs nanocomposites (d); inset of (d) is the image of the SAED pattern.

gap CdS sensitizes the wide band gap TNT, leading to that CdS/TNTs nanocomposites have the significantly enhanced visible light absorption and they are able to be “band-gap” photoexcited by visible light irradiation, by which electron–hole pairs can be generated.

To obtain the microscopic structure information of samples, the transmission electron microscopy (TEM) analysis has been carried out, as shown in Figure 3. It is observed from Figure 3a that, for blank-TNT, the uniform and nanotubular 1D structure of TNT is distinguished clearly. As to CdS/TNTs nanocomposites, we can see that the 1D nanotubular structure of

TNTs can still be well-maintained, as shown in Figure 3b,c. In the dense matrix of TNTs, the particles of CdS adhering to the wall of TNTs are observed, as evidenced from the high-resolution TEM (HRTEM) analysis in Figure 3d and typical scanning electron microscopy (SEM) analysis of CdS/TNTs nanocomposites (Figure S1a, Supporting Information). The spacing of the distinct lattice fringe in Figure 3d is measured to be 0.36 nm, corresponding to the (100) crystal plane of greenockite CdS with a hexagonal phase. The selected area electron diffraction (SAED) pattern in the inset of Figure 3d indicates that the CdS/TNTs nanocomposites possess a

Table 1. Selective Oxidation of a Range of Alcohols over Blank-TNT, CdS/TNT Nanocomposites, and Blank-CdS Photocatalysts under the Irradiation of Visible Light for 2 h

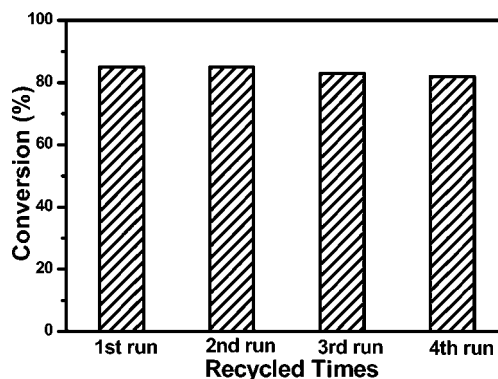
Catalyst	Substrate	Product	Conv. (%)	Sel. (%)	Substrate	Product	Conv. (%)	Sel. (%)
TNT			0.6	100			0.5	100
CdS/TNTs			85	94			82	95
CdS			13	100			15	96
TNT			0.7	99			0.6	98
CdS/TNTs			87	96			81	96
CdS			18	96			21	96
TNT			0.4	97			0.7	95
CdS/TNTs			78	93			82	94
CdS			14	95			17	94
TNT			0.4	91			0.2	90
CdS/TNTs			70	42			58	77
CdS			38	29			38	51

polycrystalline structure, which is in accordance with the result of XRD analysis. It should be particularly mentioned that the size and morphology of CdS in CdS/TNTs nanocomposites are remarkably different from those of blank-CdS (Figure S1b, Supporting Information). This suggests that the morphology and size of CdS in CdS/TNTs nanocomposites can be in situ tuned by the formation of TNTs during the one-step hydrothermal synthesis of CdS/TNTs nanocomposites. That is, TNTs act as a “dispersing template or support” to control the morphology of CdS particles during the formation of CdS/TNTs nanocomposite. In other words, the presence of TNTs is able to prevent the agglomeration of as-formed CdS particles, thus downsizing CdS particles in a small nanometer dimension.

The photocatalytic performance of CdS/TNTs nanocomposites has been evaluated by the aerobic selective oxidation of various alcohols, including benzylic alcohols and allylic alcohols, to corresponding aldehydes under visible light irradiation of 2 h under ambient conditions, that is, room temperature and atmospheric pressure. As displayed in Table 1, it can be clearly seen that CdS/TNTs nanocomposites are visible-light-active and exhibit the best and markedly much higher photocatalytic performance than blank-CdS and blank-TNT toward selective oxidation of various alcohols. Under visible light irradiation for 2 h, the conversion for benzylic alcohols to aldehydes is ca. 70–85%, whereas the conversion over the photocatalyst of blank-CdS is only ca. 13–38%. For example, the conversion of benzyl alcohol to benzaldehyde over CdS/TNTs nanocomposites is 85% under visible light irradiation for 2 h, which is much higher than 13% obtained over blank-CdS. In addition, blank-TNT shows very poor photoactivity under visible light irradiation, as reflected by the very low conversion of alcohols. This is reasonable because blank-TNT has a wide band gap, and the intrinsic limitation of visible light absorption leads to the fact that TNT by itself is not able to be “band-gap” photoexcited by visible light irradiation, which is evidenced by the UV–vis DRS in Figure

2. Time-online activity testing further corroborates the superior advantage of as-prepared CdS/TNTs nanocomposites over blank-CdS and blank-TNTs as a visible light photocatalyst for selective oxidation of benzyl alcohol to benzaldehyde, as displayed in Figure S2 (Supporting Information). Furthermore, blank experiments in the absence of catalysts and/or light show that no conversion of alcohols is observed, hence confirming that the reaction is really driven by a photocatalytic process.

In addition, we have examined the stability and reusability of highly photoactive CdS/TNTs nanocomposites in the reaction medium of benzonitrile (BN) solvent. As shown in Figure 4, during four times recycling photoactivity test for selective oxidation of benzyl alcohol over used CdS/TNTs nanocomposites, it is found that there is only a slight loss of activity as compared to that over fresh CdS/TNTs nanocomposites. Therefore, CdS/TNTs can be regarded as a highly active, stable, and reusable visible-light-driven photocatalyst for the

**Figure 4.** Recycling test of photocatalytic activity over CdS/TNTs nanocomposites toward selective oxidation of benzyl alcohol under visible light irradiation for 2 h.

selective oxidation of alcohols in the BTF solvent under ambient conditions.

To understand why CdS/TNTs nanocomposites show such a drastic photoactivity enhancement over blank-CdS and blank-TNT, the photoluminescence (PL) spectra of all of the samples have been carried out as shown in Figure 5. The PL spectra are

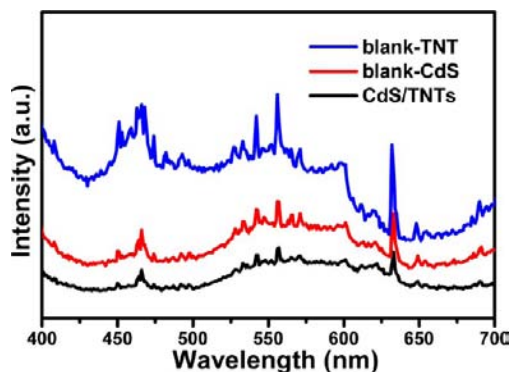


Figure 5. Photoluminescence (PL) spectra of blank-TNT, CdS/TNTs nanocomposites, and blank-CdS with an excitation wavelength of 365 nm.

often employed to study surface processes involving the electron–hole fate of the semiconductor.^{31,65–67} It is clearly seen that the PL intensity obtained over CdS/TNTs nanocomposites is much weaker than that of blank-CdS and blank-TNT, suggesting the longer lifetime of charge carriers (i.e., electron–hole pairs) photogenerated from CdS/TNTs nanocomposites. In addition, we have performed the photoelectrochemical analysis on blank-TNT and CdS/TNTs sample electrodes. Figure S3 (Supporting Information) displays the photocurrent transient response for blank-TNTs and CdS/TNT nanocomposites electrodes under visible light irradiation. As is clearly seen, the addition of CdS is able to enhance the photocurrent significantly, indicating the longer lifetime of photogenerated charge carriers over CdS/TNT as compared with blank-TNTs. Figure S4 (Supporting Information) shows the results of electrochemical impedance spectroscopy (EIS) Nyquist plots of blank-TNTs and CdS/TNT nanocomposites electrodes. Clearly, the introduction of CdS nanoparticles into the TNT matrix leads to a significantly decreased diameter of the semicircular Nyquist plot as compared to blank-TNTs, suggesting a faster charge carrier transfer rate in the CdS/TNTs nanocomposites. From the principle of photocatalysis,⁶⁸ the enhanced lifetime and transfer of charge carriers photoinduced from CdS/TNTs nanocomposites are certainly beneficial for the improved photocatalytic activity as compared to blank-CdS and blank-TNT.

In addition, we have performed the Mott–Schottky plot for blank-TNT and blank-CdS, as displayed in Figure 6. The plots with the positive slope are observed, which are consistent with the typical feature for n-type semiconductors. The flat band potential (E_{FB}) of blank-TNT and blank-CdS, as calculated from the X intercepts of the linear region, is found to be -0.55 and -0.73 V versus Ag/AgCl (equivalent to -0.35 and -0.53 V versus normal hydrogen electrode, NHE), respectively. Because the conduction band potential (E_{CB}) of blank-TNT is less negative than E_{CB} of blank-CdS, it is feasible that photogenerated electrons from CdS in CdS/TNTs nanocomposites upon visible light irradiation are able to transfer from the conduction band (CB) of CdS to the CB of TNTs when they

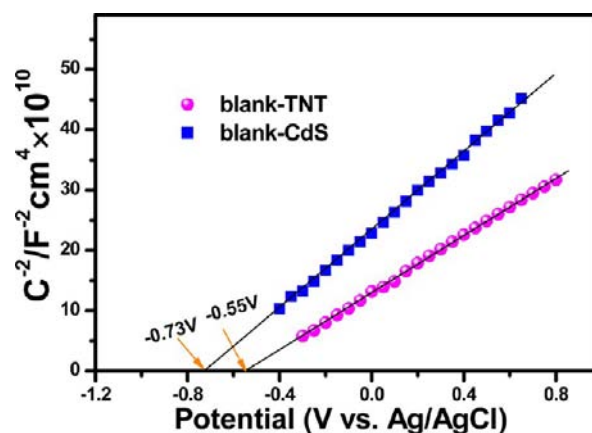


Figure 6. Mott–Schottky plot for blank-TNT and blank-CdS in 0.2 M Na_2SO_4 aqueous solution (pH = 6.8).

are coupled with a good interfacial contact, which thus contributes to separating the charge carriers and prolonging the fate of electron–hole pairs of CdS/TNTs nanocomposites upon visible light irradiation. This consequently leads to the remarkable enhancement of visible light photoactivity as observed for the above selective oxidation of alcohols over CdS/TNTs nanocomposites.

To further understand the significant photoactivity enhancement of CdS/TNTs nanocomposites, the surface area and porosity of all samples have been investigated, as displayed in Figure S5 (Supporting Information). The specific Brunauer–Emmett–Teller (BET) surface area of blank-TNT, CdS/TNTs nanocomposites, and blank-CdS is determined to be ca. 379, 110, and $10 \text{ m}^2/\text{g}$, respectively. Apparently, the surface area of CdS/TNTs nanocomposites is 11 times that of blank-CdS, but still 3 times lower than that of blank-TNT. Furthermore, the average pore diameter and pore volume are 5 nm and $0.97 \text{ cm}^3/\text{g}$ for blank-TNT, 5 nm and $0.19 \text{ cm}^3/\text{g}$ for CdS/TNTs nanocomposites, and 3 nm and $0.07 \text{ cm}^3/\text{g}$ for blank-CdS, respectively. Thus, the surface area and pore volume of CdS/TNTs nanocomposites are both much higher than those of blank-CdS, but lower than those of blank-TNT, implying that the adsorption capacity toward substrate alcohols over CdS/TNTs should be higher than that of blank-CdS, but lower than that of blank-TNT, as is evidenced by adsorption experiments in the dark for various alcohols over all of the samples (Figure S6, Supporting Information). Because TNTs cannot be “band-gap” photoexcited under visible light irradiation, its highest surface area among these three samples should not be considered in affecting the overall photoactivity order. On the contrary, for blank-CdS and CdS/TNTs nanocomposites that can both be “band-gap” photoexcited under visible light irradiation, the higher surface area and higher adsorption capacity toward alcohols over CdS/TNTs nanocomposites than blank-CdS can cause the accumulation of alcohol concentration over the catalyst surface, therefore being the other beneficial factor contributing to the photoactivity enhancement.^{57,62} To further understand the effect of surface area on promoting the photoactivity, the sample of blank-CdS nanoparticles supported on high-surface-area SBA-15 has been tested for its photoactivity toward oxidation of benzyl alcohol under visible light irradiation. As reflected by this controlled experiment in Figure S7 (Supporting Information), it is obvious that CdS/SBA-15 exhibits a higher photoactivity than blank-CdS, but its photoactivity is still much lower than CdS/TNTs under

identical reaction conditions. This result suggests that the increased surface area is just one factor contributing to the photoactivity enhancement of CdS/TNTs as compared to blank-CdS. Other factors, for example, the improved lifetime and transfer of photogenerated charge carriers induced by the hybridized structure of the CdS/TNTs nanocomposite, together contribute to the overall photoactivity enhancement of CdS/TNTs toward photocatalytic oxidation of alcohols under visible light irradiation. In addition, to study the crystallite size effect of CdS particles on improving the photoactivity, we have chosen commercial nano CdS, which has an average crystallite size of about 27 nm according to calculation from the (002) peak of the XRD pattern by the Scherrer formula and the same crystalline phase as blank-CdS (Figure S8, Supporting Information), and tested its photoactivity for selective oxidation of benzyl alcohol under identical reaction conditions. The data are displayed in Figure S9 (Supporting Information). Obviously, commercial nano CdS with a smaller crystallite size exhibits a higher photoactivity than blank-CdS with a larger crystallite size of about 49 nm. Therefore, the smaller size of CdS in the CdS/TNTs composites than that of blank-CdS is also one factor contributing to the photoactivity enhancement.

Therefore, on the basis of the above discussion, we ascribe the significantly enhanced visible light photoactivity of CdS/TNTs nanocomposites over blank-CdS and blank-TNT to the following three integrative factors. The first one is the different morphology and size of CdS in CdS/TNTs nanocomposites from that of blank-CdS. The second one is the prolonged lifetime of electron–hole pairs photogenerated from CdS in CdS/TNTs nanocomposites as compared to blank-CdS under visible light irradiation. The third one is the higher surface area and adsorption capacity toward alcohols of CdS/TNTs nanocomposites than that of blank-CdS.

To understand the possible reaction mechanism for photocatalytic selective oxidation of alcohols over CdS/TNTs nanocomposites, we have further performed a series of controlled experiments.^{24,61,65,66,69} The data are shown in Figure 7. The experiment carried out in the inert nitrogen (N_2) atmosphere shows that only trace conversion of benzyl alcohol

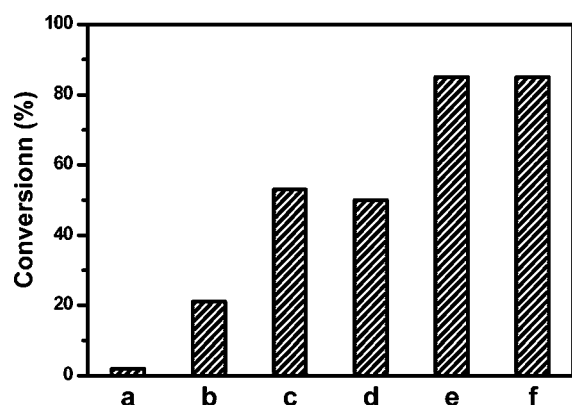


Figure 7. Controlled experiments for selective oxidation of benzyl alcohol over CdS/TNTs nanocomposites in the BTF solvent under visible light irradiation for 2h: (a) reaction with N_2 -saturated atmosphere, (b) reaction with benzoquinone (BQ) as scavenger for superoxide radicals, (c) reaction with $AgNO_3$ as scavenger for electrons, (d) reaction with ammonium oxalate (AO) as scavenger for holes, (e) reaction with *tert*-butyl alcohol (TBA) as scavenger for hydroxyl radicals, (f) reaction in the absence of radical scavengers.

is obtained (entry a in Figure 7), demonstrating that oxygen is the primary oxidant during the photocatalytic oxidation of alcohols over CdS/TNTs nanocomposites under visible light irradiation. When the radical scavenger of benzoquinone (BQ) for superoxide radical ($O_2^{\bullet-}$) species is added into the reaction system, the photocatalytic reaction is remarkably inhibited (entry b in Figure 7). Furthermore, when the scavenger of $AgNO_3$ for electrons is added, the photocatalytic reaction is also decreased (entry c in Figure 7). A similar suppression phenomenon for the photocatalytic reaction is also observed when the ammonium oxalate (AO) scavenger for holes (entry d in Figure 7) is added to the reaction system. These suggest that the photocatalytic oxidation of alcohols over CdS/TNTs nanocomposites is primarily driven by photogenerated electrons, holes, and activated oxygen (e.g., $O_2^{\bullet-}$). The presence of superoxide radicals ($O_2^{\bullet-}$) is confirmed by the electron spin resonance (ESR) analysis, as displayed in Figure S10 (Supporting Information). It should be mentioned that, in the BTF solvent, the strong and nonselective hydroxyl radicals ($\bullet OH$) are not formed, as also observed in previous works.^{24,58–62,65,66,69} Indeed, the addition of *tert*-butyl alcohol as scavenger for $\bullet OH$ does not play an inhibition effect on the conversion of benzyl alcohol, as evidenced in entry e in Figure 7, indicating the absence of $\bullet OH$ radicals in the BTF solvent.^{24,58–62,65,66,69}

On the basis of the above experiments, a tentative photocatalytic reaction mechanism for selective oxidation of alcohols to corresponding aldehydes over CdS/TNTs nanocomposites can be schematically proposed in Figure 8. Under the irradiation of

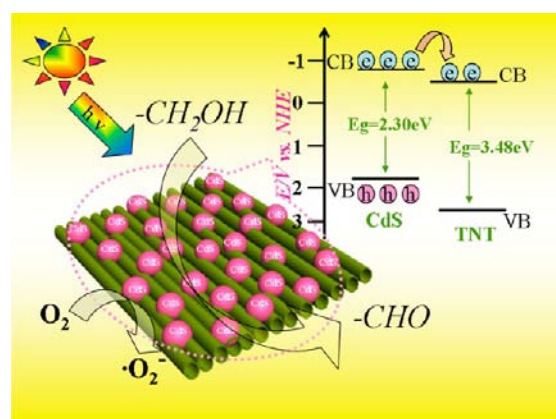


Figure 8. Schematic diagram of the proposed mechanism for selective oxidation of alcohols to corresponding aldehydes over the CdS/TNTs nanocomposites under the visible light irradiation.

visible light, the electrons are excited from the valence band (VB) of CdS nanoparticles in CdS/TNTs nanocomposites to its conduction band (CB), thereby forming the photoactive electron–hole pairs. Simultaneously, the photogenerated electrons can fleetly transfer to the CB of TNTs because of the match of CB potential position and intimate contact between CdS nanoparticles and TNTs, which can be further trapped by molecular oxygen in the reaction system to activate molecular oxygen (e.g., the formation of superoxide radicals), thus efficiently inhibiting the recombination of electron–hole pairs and prolonging the lifetime of charge carriers. The alcohols can be rapidly adsorbed on the CdS/TNTs nanocomposites owing to the large surface area and adsorption capacity and then oxidized by the active species, for example,

holes and activated oxygen, forming the corresponding aldehydes.

CONCLUSION

In summary, we have synthesized CdS–1D titanate nanotubes (CdS/TNTs) nanocomposites via a facile one-step in situ hydrothermal method during which the formation of the 1D nanostructure of TNT and CdS nanoparticles is obtained simultaneously. As compared to blank-CdS, the morphology of CdS can be tuned by the formation of TNTs in such an in situ synthesis of CdS/TNTs nanocomposites while the 1D nanostructure of TNTs is not influenced. Furthermore, CdS/TNTs nanocomposites exhibit the best and much higher photocatalytic performance among these three samples toward aerobic selective oxidation of various alcohols under visible light irradiation. The remarkably enhanced photocatalytic performance for CdS/TNTs nanocomposites can be attributed to three integrative factors. The first one is the different morphology and size of CdS in the CdS/TNTs nanocomposites from blank-CdS. The second one is the prolonged lifetime of charge carriers photoexcited from CdS in CdS/TNTs nanocomposites as compared to blank-CdS under visible light irradiation. The third one is the higher surface area and adsorption capacity toward alcohols of CdS/TNTs nanocomposites than that of blank-CdS. This work is the first time to utilize CdS/1D TNTs nanocomposites as a visible light photocatalyst for selective organic synthesis under ambient conditions. It is expected that our work could boost further interest in fabrication of various 1D TNT architecture-based composite materials and their application to visible-light-driven selective organic transformations.

ASSOCIATED CONTENT

Supporting Information

Additional data, including SEM images, size distribution of CdS particles, time-online photocatalytic activity, N₂ adsorption-desorption isotherms and corresponding pore size distribution, adsorption experiments in the dark, photoelectrochemical analysis, XRD patterns of commercial nano CdS and blank-CdS, control photoactivity test over CdS/SBA-15 and commercial nano CdS, and ESR results. This material is available free of charge via the Internet at <http://pubs.acs.org>.

AUTHOR INFORMATION

Corresponding Author

*Tel/Fax: +86 591 22866126. E-mail: zrtang@fzu.edu.cn.

Notes

The authors declare no competing financial interest.

ACKNOWLEDGMENTS

The support by the National Natural Science Foundation of China (NSFC) (20903022, 20903023, 21173045), the Science and Technology Development of Foundation of Fuzhou University (2009-XQ-10), the Open Fund of Photocatalysis of Fuzhou University (0380038004), and the Program for Returned High-Level Overseas Chinese Scholars of Fujian province is gratefully acknowledged.

REFERENCES

(1) Huynh, W. U.; Dittmer, J. J.; Alivisatos, A. P. *Science* **2002**, *295*, 2425–2427.

(2) Tian, B. Z.; Zheng, X. L.; Kempa, T. J.; Fang, Y.; Yu, N. F.; Yu, G. H.; Huang, J. L.; Lieber, C. M. *Nature* **2007**, *449*, 885–U8.

(3) Hochbaum, A. I.; Chen, R. K.; Delgado, R. D.; Liang, W. J.; Garnett, E. C.; Najarian, M.; Majumdar, A.; Yang, P. D. *Nature* **2008**, *451*, 163–U5.

(4) Gautam, U. K.; Fang, X. S.; Bando, Y.; Zhan, J. H.; Golberg, D. *ACS Nano* **2008**, *2*, 1015–1021.

(5) Wang, J. F.; Gudiksen, M. S.; Duan, X. F.; Cui, Y.; Lieber, C. M. *Science* **2001**, *293*, 1455–1457.

(6) McPhillips, J.; Murphy, A.; Jonsson, M. P.; Hendren, W. R.; Atkinson, R.; Hook, F.; Zayats, A. V.; Pollard, R. J. *ACS Nano* **2010**, *4*, 2210–2216.

(7) Mor, G. K.; Varghese, O. K.; Paulose, M.; Shankar, K.; Grimes, C. A. *Sol. Energy Mater. Sol. Cells* **2006**, *90*, 2011–2075.

(8) Chen, X.; Mao, S. S. *Chem. Rev.* **2007**, *107*, 2891–2959.

(9) Wang, Y. L.; Jiang, X. C.; Xia, Y. N. *J. Am. Chem. Soc.* **2003**, *125*, 16176–16177.

(10) Wang, Z. L. *ACS Nano* **2008**, *2*, 1987–1992.

(11) Wang, L. S.; Xiao, M. W.; Huang, X. J.; Wu, Y. D. *J. Hazard. Mater.* **2009**, *161*, 49–54.

(12) Xue, W.; Zhang, G.; Xu, X.; Yang, X.; Liu, C.; Xu, Y. *Chem. Eng. J.* **2011**, *167*, 397–402.

(13) Costa, L. L.; Prado, A. G. S. *J. Photochem. Photobiol., A* **2009**, *201*, 45–49.

(14) Hou, L.-R.; Yuan, C.-Z.; Peng, Y. *J. Hazard. Mater.* **2007**, *139*, 310–315.

(15) Geng, J. Q.; Jiang, Z. Y.; Wang, Y. B.; Yang, D. *Scr. Mater.* **2008**, *59*, 352–355.

(16) Liu, Z. H.; Chen, J. Z.; Zhang, Y. Y.; Wu, L. P.; Li, X. J. *Mater. Chem. Phys.* **2011**, *128*, 1–5.

(17) Xu, S. P.; Ng, J. W.; Zhang, X. W.; Bai, H. W.; Sun, D. D. *Colloids Surf., A* **2011**, *379*, 169–175.

(18) Tang, Z.-R.; Li, F.; Zhang, Y.; Fu, X.; Xu, Y.-J. *J. Phys. Chem. C* **2011**, *115*, 7880–7886.

(19) Xu, S. P.; Du, A.; Liu, J. C.; Ng, J. W.; Sun, D. D. *Int. J. Hydrogen Energy* **2011**, *36*, 6560–6568.

(20) Xu, S. P.; Ng, J. W.; Du, A.; Liu, J. C.; Sun, D. D. *Int. J. Hydrogen Energy* **2011**, *36*, 6538–6545.

(21) Li, C. L.; Yuan, J.; Han, B. Y.; Jiang, L.; Shangguan, W. F. *Int. J. Hydrogen Energy* **2010**, *35*, 7073–7079.

(22) Jia, F. Z.; Yao, Z. P.; Jiang, Z. H.; Li, C. X. *Catal. Commun.* **2011**, *12*, 497–501.

(23) Khan, M. A.; Jung, H.-T.; Yang, O.-B. *J. Phys. Chem. B* **2006**, *110*, 6626–6630.

(24) Tang, Z. R.; Zhang, Y. H.; Xu, Y. J. *ACS Appl. Mater. Interfaces* **2012**, *4*, 1512–1520.

(25) Khan, M. A.; Yang, O. B. *Catal. Today* **2009**, *146*, 177–182.

(26) Liu, Z. Y.; Pestic, B.; Raja, K. S.; Rangaraju, R. R.; Misra, M. *Int. J. Hydrogen Energy* **2009**, *34*, 3250–3257.

(27) Ghicov, A.; Macak, J. M.; Tsuchiya, H.; Kunze, J.; Haeublein, V.; Frey, L.; Schmuki, P. *Nano Lett.* **2006**, *6*, 1080–1082.

(28) Wang, C. L.; Sun, L.; Yun, H.; Li, J.; Lai, Y. K.; Lin, C. J. *Nanotechnology* **2009**, *20*, 295601–295606.

(29) Chen, S. G.; Paulose, M.; Ruan, C.; Mor, G. K.; Varghese, O. K.; Kouzoudis, D.; Grimes, C. A. *J. Photochem. Photobiol., A* **2006**, *177*, 177–184.

(30) Shin, K.; Seok, S. I.; Im, S. H.; Park, J. H. *Chem. Commun.* **2010**, *46*, 2385–2387.

(31) Baker, D. R.; Kamat, P. V. *Adv. Funct. Mater.* **2009**, *19*, 805–811.

(32) Baker, D. R.; Kamat, P. V. *J. Phys. Chem. C* **2009**, *113*, 17967–17972.

(33) Xie, Y.; Ali, G.; Yoo, S. H.; Cho, S. O. *ACS Appl. Mater. Interfaces* **2010**, *2*, 2910–2914.

(34) Sun, W. T.; Yu, Y.; Pan, H. Y.; Gao, X. F.; Chen, Q.; Peng, L. M. *J. Am. Chem. Soc.* **2008**, *130*, 1124–1125.

(35) Bai, J.; Li, J. H.; Liu, Y. B.; Zhou, B. X.; Cai, W. M. *Appl. Catal., B* **2010**, *95*, 408–413.

- (36) Kim, J. C.; Choi, J.; Lee, Y. B.; Hong, J. H.; Lee, J. I.; Yang, J. W.; Lee, W. I.; Hur, N. H. *Chem. Commun.* **2006**, 5024–5026.
- (37) Gao, X. F.; Li, H. B.; Sun, W. T.; Chen, Q.; Tang, F. Q.; Peng, L. M. *J. Phys. Chem. C* **2009**, *113*, 7531–7535.
- (38) Banerjee, S.; Mohapatra, S. K.; Das, P. P.; Misra, M. *Chem. Mater.* **2008**, *20*, 6784–6791.
- (39) Lin, C. J.; Yu, Y. H.; Liou, Y. H. *Appl. Catal., B* **2009**, *93*, 119–125.
- (40) Kongkanand, A.; Tvrđy, K.; Takechi, K.; Kuno, M.; Kamat, P. V. *J. Am. Chem. Soc.* **2008**, *130*, 4007–4015.
- (41) Zhang, H.; Quan, X.; Chen, S.; Yu, H. T.; Ma, N. *Chem. Mater.* **2009**, *21*, 3090–3095.
- (42) Seabold, J. A.; Shankar, K.; Wilke, R. H. T.; Paulose, M.; Varghese, O. K.; Grimes, C. A.; Choi, K. S. *Chem. Mater.* **2008**, *20*, 5266–5273.
- (43) Yang, L. X.; Chen, B. B.; Luo, S. L.; Li, J. X.; Liu, R. H.; Cai, Q. Y. *Environ. Sci. Technol.* **2010**, *44*, 7884–7889.
- (44) Chen, Y. B.; Wang, L. Z.; Lu, G. Q.; Yao, X. D.; Guo, L. J. *J. Mater. Chem.* **2011**, *21*, 5134–5141.
- (45) Zhou, Q.; Fu, M. L.; Yuan, B. L.; Cui, H. J.; Shi, J. W. *J. Nanopart. Res.* **2011**, *13*, 6661–6672.
- (46) Kukovec, A.; Hodos, M.; Konya, Z.; Kiricsi, I. *Chem. Phys. Lett.* **2005**, *411*, 445–449.
- (47) Hodos, M.; Horváth, E.; Haspel, H.; Kukovec, Á.; Kónya, Z.; Kiricsi, I. *Chem. Phys. Lett.* **2004**, *399*, 512–515.
- (48) Xing, C.; Jing, D.; Liu, M.; Guo, L. *Mater. Res. Bull.* **2009**, *44*, 442–445.
- (49) Zhang, Y. J.; Wu, Y. P.; Wang, Z. H.; Hu, Y. R. *Rare Met. Mater. Eng.* **2009**, *38*, 1514–1517.
- (50) Yin, Y.; Jin, Z.; Hou, F. *Nanotechnology* **2007**, *18*, 495608.
- (51) Palmisano, G.; Augugliaro, V.; Pagliaro, M.; Palmisano, L. *Chem. Commun.* **2007**, 3425–3437.
- (52) Palmisano, G.; Garcia-Lopez, E.; Marci, G.; Loddo, V.; Yurdakal, S.; Augugliaro, V.; Palmisano, L. *Chem. Commun.* **2010**, *46*, 7074–7089.
- (53) Higashimoto, S.; Suetsugu, N.; Azuma, M.; Ohue, H.; Sakata, Y. *J. Catal.* **2010**, *274*, 76–83.
- (54) Pillai, U. R.; Sahle-Demessie, E. *J. Catal.* **2002**, *211*, 434–444.
- (55) Shiraishi, Y.; Hirai, T. *J. Photochem. Photobiol., C* **2008**, *9*, 157–170.
- (56) Zhang, N.; Zhang, Y.; Pan, X.; Fu, X.; Xu, Y. J. *Sci. China: Chem.* **2011**, *41*, 1097–1111.
- (57) Maldotti, A.; Molinari, A.; Amadelli, R. *Chem. Rev.* **2002**, *102*, 3811–3836.
- (58) Zhang, Y.; Tang, Z.-R.; Fu, X.; Xu, Y.-J. *ACS Nano* **2011**, *5*, 7426–7435.
- (59) Zhang, N.; Fu, X.; Xu, Y.-J. *J. Mater. Chem.* **2011**, *21*, 8152–8158.
- (60) Zhang, N.; Liu, S.; Fu, X.; Xu, Y.-J. *J. Phys. Chem. C* **2011**, *115*, 22901–22909.
- (61) Zhang, Y.; Zhang, N.; Tang, Z.-R.; Xu, Y.-J. *Chem. Sci.* **2012**, *3*, 2812–2822.
- (62) Zhang, N.; Zhang, Y.; Pan, X.; Fu, X.; Liu, S.; Xu, Y.-J. *J. Phys. Chem. C* **2011**, *115*, 23501–23511.
- (63) Ou, H.-H.; Liao, C.-H.; Liou, Y.-H.; Hong, J.-H.; Lo, S.-L. *Environ. Sci. Technol.* **2008**, *42*, 4507–4512.
- (64) Lee, C.-K.; Wang, C.-C.; Lyu, M.-D.; Juang, L.-C.; Liu, S.-S.; Hung, S.-H. *J. Colloid Interface Sci.* **2007**, *316*, 562–569.
- (65) Liu, S.; Zhang, N.; Tang, Z.-R.; Xu, Y.-J. *ACS Appl. Mater. Interfaces* **2012**, *4*, 6378–6385.
- (66) Zhang, Y.; Zhang, N.; Tang, Z.-R.; Xu, Y.-J. *ACS Nano* **2012**, *6*, 9777–9789.
- (67) Xu, Y.-J.; Zhuang, Y.; Fu, X. *J. Phys. Chem. C* **2010**, *114*, 2669–2676.
- (68) Zhang, Q.; Deng, W.; Wang, Y. *Phys. Chem. Chem. Phys.* **2013**, *15*, 2632–2649.
- (69) Zhang, N.; Zhang, Y.; Yang, M.-Q.; Tang, Z.-R.; Xu, Y.-J. *J. Catal.* **2013**, *299*, 210–221.